

Mosaic spin models with topological order

S. Yang,¹ D. L. Zhou,² and C. P. Sun¹

¹*Institute of Theoretical Physics, Chinese Academy of Sciences, Beijing 100080, China*

²*Institute of Physics, Chinese Academy of Sciences, Beijing 100080, China*

(Received 9 October 2007; published 9 November 2007)

We study a class of two-dimensional spin models with the Kitaev-type couplings in mosaic structure lattices to implement topological orders. We show that they are exactly solvable by reducing them to some free Majorana fermion models with gauge symmetries. The typical case with a 4-8-8 close packing is investigated in detail to display the quantum phases with Abelian and non-Abelian anyons. Its topological properties characterized by Chern numbers are revealed through the edge modes of its spectrum.

DOI: 10.1103/PhysRevB.76.180404

PACS number(s): 75.10.Jm, 05.30.Pr, 71.10.Pm

INTRODUCTION

The phenomenon of emergence (such as a phase transition) in a condensed matter system is usually understood according to the Landau symmetry-breaking theory (LSBT).¹ There also exists a new kind of order called “topological order”¹⁻⁵ which cannot be described in the frame of the LSBT (e.g., fractional quantum Hall effect). The study of topological order in theoretical and experimental aspects has been an active area of research.²⁻¹⁵ Since local perturbations hardly destroy the topological properties, such topologically ordered states show exciting potential to encode and process quantum information robustly.² Therefore it is significant and challenging to find more exactly solvable models showing various topological orders.

In this Rapid Communication, the Kitaev’s honeycomb model² is generalized to the general mosaic spin models with different two-dimensional Bravais lattices of complex unit cells. Then we study the 4-8-8 case in detail to reveal the general and special properties of mosaic spin models.

Our mosaic spin models are constructed with the basic block shown in Fig. 1(a), which is a vertex with three different types of spin couplings along x - (black solid link), y - (blue dotted link), and z - (red double link) directions, respectively. In spite of the lattice symmetry, numerous spin models can be built based on this basic block. However, taking translational symmetry and rotational symmetry as much as possible into account, we regard each basic block as the common vertex of three isogons with n_1 , n_2 , and n_3 edges, so there are only four kinds of mosaic spin models¹⁶ illustrated in Figs. 1(b)–1(e), called n_1 - n_2 - n_3 mosaic models.

Obviously, the 6-6-6 mosaic model is just Kitaev’s honeycomb model.² Here, we remark that for given n_1 , n_2 , and n_3 , there exist some unequivalent kinds of plane arrangement of x links, y links, and z links, but we only illustrate one of them in Fig. 1. The general Hamiltonian of all mosaic spin models reads as

$$H = - \sum_{u=x,y,z} J_u \sum_{(j,k) \in S(u)} \sigma_j^u \sigma_k^u, \quad (1)$$

where $S(u)$ is the set of links with u -direction couplings.

PERTURBATION THEORY STUDY AND ABELIAN ANYONS

First, we study the 4-8-8 mosaic model as a typical illustration in detail. To see its topological properties, we first analyze its low energy excitations when the system is initially spontaneously polarized with the strong Ising interaction $H_0 = -J_z \sum_{z \text{ links}} \sigma_j^z \sigma_k^z$. The ground energy of H_0 is $E_0 = -NJ_z$, where N is the number of z links. For larger J_z in comparison with J_x and J_y , we regard the transverse part $V = H - H_0$ as a perturbation and then prove that the obtained effective Hamiltonian H_{eff} just describes Kitaev’s toric code model,² which supports many topological issues of the original mosaic spin model.

The ground eigenstates of H_0 are highly degenerate, where each two spins connected by a z link can be either $|\uparrow\uparrow\rangle$ or $|\downarrow\downarrow\rangle$. The fusion projection² Y_l^\dagger can map the l th aligned spin pair $|m, m\rangle_l$ to an effective spin $|m\rangle_l$ ($m = \uparrow$ or \downarrow), i.e., $Y_l^\dagger |m, m\rangle_l = |m\rangle_l$. We use the fusion projection and the Green function formalism to calculate the

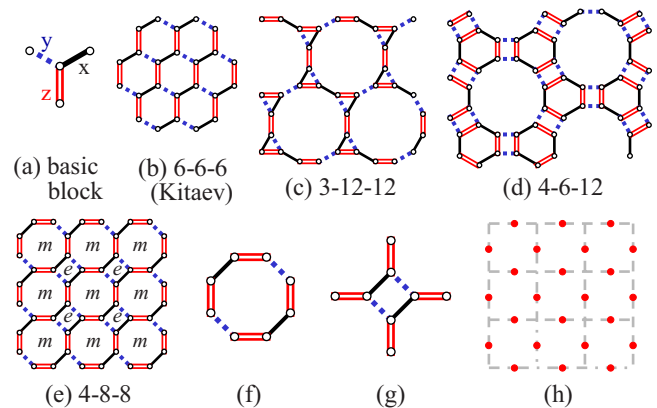


FIG. 1. (Color online) (a) Basic block for mosaic spin models, which consists of three branches with x - (black solid link), y - (blue dotted link), and z - (red double link) type couplings. (b) 6-6-6 mosaic model, i.e., Kitaev’s honeycomb model. (c) 3-12-12 mosaic model. (d) 4-6-12 mosaic model. (e) 4-8-8 mosaic model, e vortices lie on squares while m vortices lie on octagons. (f) and (g) The possible nonconstant terms of the effective Hamiltonian are obtained by flipping four spin pairs around an octagon (f) and a square (g). (h) Kitaev’s toric code model is the effective model of the 4-8-8 mosaic model when $|J_z| \gg |J_x|, |J_y|$.

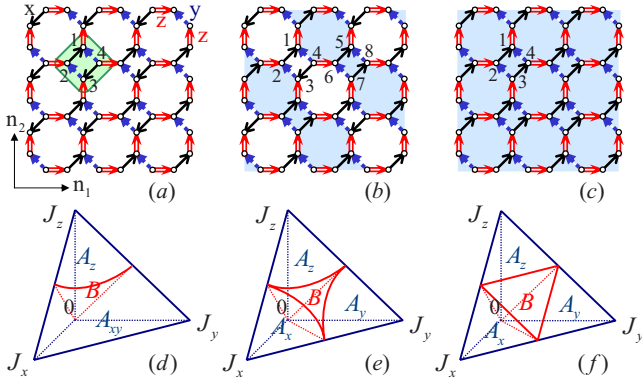


FIG. 2. (Color online) (a)–(c) 4-8-8 mosaic spin models in (a) vortex-free (VF) sector, (b) vortex-half occupied (VHO) sector, and (c) vortex-full occupied (VFO) sector. (d)–(f) The corresponding phase graphs of the above lattices with gapless phase B and gapped phases A : (d) VF, (e) VHO, and (f) VFO.

effective Hamiltonian $H_{eff} = \sum_{l=0}^{\infty} H_{eff}^{(l)} = E_0 + Y^\dagger V [1 + G_0(E_0) + G_0(E_0) V G_0(E_0)] V Y + \dots$ where $G_0(E_0) = (E_0 - H_0)^{-1}$. We first obtain the constant zeroth order one, the vanishing first order, and third order ones. Here, each terms $\sigma_j^x \sigma_k^x$ or $\sigma_j^y \sigma_k^y$ in V flips two spins, increasing the energy by $4J_z$. Up to the second order perturbation, one V flips two spins and the other V flips them back, giving $H_{eff}^{(2)} = -N(J_x^2 + J_y^2)/(4J_z)$ as a constant. As shown in Figs. 1(f) and 1(g), we take two $\sigma_j^x \sigma_k^x$ and two $\sigma_j^y \sigma_k^y$ from four V around one octagon or one quatrefoil in a particular order. Taking all the $2 \times 4! = 48$ possible cases into account, we obtain the fourth order effective Hamiltonian

$$H_{eff}^{(4)} = -\frac{J_x^2 J_y^2}{16J_z^3} \left(5 \sum_O \sigma_l^y \sigma_r^y \sigma_u^y \sigma_d^y + \sum_Q \sigma_l^z \sigma_r^z \sigma_u^z \sigma_d^z \right), \quad (2)$$

where the constant term was dropped, and O and Q represent the octagon and quatrefoil in the two-dimensional (2D) lattice. Up to a unitary transformation for spin rotation $\sigma^y \rightarrow \sigma^z$, $\sigma^z \rightarrow \sigma^x$, $\sigma^x \rightarrow \sigma^y$, the above Hamiltonian represents the Kitaev's toric code model.² Thus the above fusion projection constructs a new Bravais lattice illustrated in Fig. 1(h) with the effective spins laying on its links. Considering the Kitaev model (2) possesses rich topological features characterized by m and e anyons, we conclude that m particles live on octagons while e particles live on squares in our model with original spin representation.

MAJORANA FERMION MAPPING WITH \mathbb{Z}_2 -GAUGE SYMMETRY

The 4-8-8 mosaic model consists of four equivalent simple sublattices, and a unit cell [see the green rhombus tablet in Fig. 2(a)] contains each of four kinds of vortices referred to as 1, 2, 3, and 4. According to Kitaev,² we use the Majorana fermion operators to represent Pauli operators as $\sigma^x = ib^x c$, $\sigma^y = ib^y c$, and $\sigma^z = ib^z c$, where Majorana operators b^x, b^y, b^z , and c satisfy $\alpha^2 = 1$, $\alpha\beta = -\beta\alpha$ for $\alpha, \beta \in \{b^x, b^y, b^z, c\}$ and $\alpha \neq \beta$. Then, the Hamiltonian (1) can be rewritten as $H = \sum_{j,k} \frac{1}{2} G_{jk} c_j c_k$, where the operator-valued cou-

pling $G_{jk} \equiv iJ_u Z_{jk}$ ($u=x, y, z$) if $(j, k) \in S(u)$; $G_{jk} = 0$ when $(j, k) \notin S(u)$. Here, a link (j, k) determines a type of coupling $u = u(j, k)$. Due to the vanishing anticommutator of b_j^u and b_k^u , we have $Z_{jk} = -Z_{kj}$ for $j \neq k$.

For each site, the above-mentioned Majorana operators act on a 4D space, but the physical subspace is only 2D. Thus we need to invoke a gauge transformation of the \mathbb{Z}_2 group to project the extended space into the physical subspace through the projection operator $D = b^x b^y b^z c$: $|\psi\rangle$ belongs to the physical subspace if and only if $D|\psi\rangle = |\psi\rangle$. With this physical projection, some eigenstates of H can be found exactly because G_{jk} lays on the center of an Abelian algebra generated by Z_{jk} with $[Z_{jk}, H] = 0$ and $[Z_{jk}, Z_{ml}] = 0$. Since $(Z_{jk})^2 = 1$, $Z_{jk} = ib^u b_k^u$ generates a \mathbb{Z}_2 group and its eigenvalues are $z_{jk} = \pm 1$. Therefore, $\{Z_{jk}, I | (j, k) \in S(u), u=x, y, z\}$ generate the symmetry group $\mathbb{Z}_2 \otimes \mathbb{Z}_2 \otimes \dots \otimes \mathbb{Z}_2$ of the model; the whole Hilbert space is then decomposed according to the direct sum of some irreducible representations, and each irreducible sector is characterized by $\{z_{jk} | (j, k) \in S(u), u=x, y, z\}$, i.e., the directions shown in Figs. 2(a)–2(c).

Obviously, in each irreducible representation space, we can reduce the Hamiltonian (1) into a quadratic form, which represents an effective Hamiltonian of free fermions for a given vortex arrangement. To characterize the vortex configuration, we introduce square and octagon plaquette operators $W_p^{(4)} = \sigma_1^z \sigma_2^z \sigma_3^z \sigma_4^z$ and $W_p^{(8)} = \sigma_1^y \sigma_2^y \sigma_3^x \sigma_4^x \sigma_5^y \sigma_6^y \sigma_7^x \sigma_8^x$ or

$$W_p^{(4)} = - \prod_{(j,k) \in \partial p(4)} Z_{jk}, \quad W_p^{(8)} = - \prod_{(j,k) \in \partial p(8)} Z_{jk}, \quad (3)$$

where $\partial p(4)$ and $\partial p(8)$ represent the sets of boundary links of square and octagon plaquettes with label p ; the (j, k) links are ordered clockwise around the plaquette. The operators $W_p^{(j)}$ ($j=4, 8$) commute with each other, $[W_p^{(j)}, H] = 0$, $W_p^{(4)2} = W_p^{(8)2} = I$, and thus each plaquette operator has two eigenvalues $w_p = \pm 1$. A plaquette with $w_p = 1$ is a vortex-free plaquette while $w_p = -1$ corresponds to a vortex. In the following we will show that different arrangements of vortices result in different phase graphs and different energy spectrums.

4-8-8 MOSAIC MODEL IN DIFFERENT VORTEX-OCCUPIED SECTORS

Let us denote the site index j in detail by (s, λ) , where s refers to a unit cell, and λ to a position type inside the cell. The Hamiltonian then reads $H = \sum_{s, \lambda, t, \mu} G_{s\lambda, t\mu} c_{s\lambda} c_{t\mu} / 2$. Due to the translational invariance of the lattice along the unit direction vectors $\mathbf{n}_1 = (1, 0)$, $\mathbf{n}_2 = (0, 1)$, $G_{s\lambda, t\mu}$ actually depends on λ, μ and $t-s$, and thus $\exp[i\mathbf{q} \cdot (\mathbf{r}_t - \mathbf{r}_s)] G_{s\lambda, t\mu} = \exp(i\mathbf{q} \cdot \mathbf{r}_t) G_{0\lambda, t\mu}$. To study the spectral structure of the system, we invoke the generic fermion operator $a_{\mathbf{q}, \mu} = \sum_t e^{i\mathbf{q} \cdot \mathbf{r}_t} c_{t\mu} / \sqrt{2N}$ where N is the total number of the unit cells and $a_{\mathbf{p}, \mu} a_{\mathbf{q}, \lambda}^\dagger + a_{\mathbf{q}, \lambda}^\dagger a_{\mathbf{p}, \mu} = \delta_{\mathbf{p}\mathbf{q}} \delta_{\mu\lambda}$. $\tilde{G}_{\lambda\mu}(\mathbf{q})$ is the Fourier transformation of $G_{0\lambda, t\mu}$. In the momentum space, the fermion representation of the Hamiltonian reads

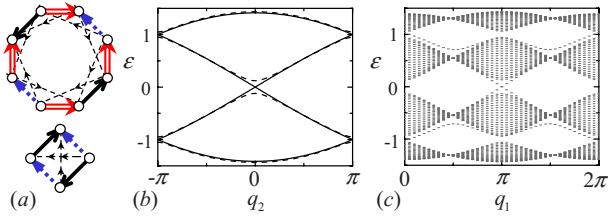


FIG. 3. (Color online) (a) Thin dashed arrows describe the effective second nearest-neighbor interactions between fermions and the corresponding gauge induced by a magnetic field. (b) Profile graph of an energy spectrum with $J_x=J_y=1$, $J_z=\sqrt{2}$ along the $q_1=\pi$ axis in the absence (solid lines) and presence (dashed lines) of a magnetic field. (c) Energy spectrum of the above system with finite size along the \mathbf{n}_2 direction in the magnetic field. Two chiral edge modes crossing at $E=0$ correspond to Chern number ± 1 .

$$H = \frac{1}{2} \sum_{\mathbf{q}} A_{\mathbf{q}}^{\dagger} \tilde{G}(\mathbf{q}) A_{\mathbf{q}}. \quad (4)$$

Case I. In the vortex-free (VF) sector, we choose a particular direction ($z_{jk}=+1$ or -1) for each link [see Fig. 2(a)], so that translational symmetry holds and $w_p^{(4)}=w_p^{(8)}=1$ for all plaquettes. Since $A_{\mathbf{q}}^{\dagger}=(a_{\mathbf{q},1}^{\dagger}, a_{\mathbf{q},2}^{\dagger}, a_{\mathbf{q},3}^{\dagger}, a_{\mathbf{q},4}^{\dagger})$, we have the 4×4 spectral matrix $\tilde{G}(\mathbf{q})=\tilde{G}_{VF}$ or

$$\tilde{G}_{VF} = \begin{pmatrix} J_x \sigma^y & -iJ_y \sigma^x + iJ_z \alpha \\ iJ_y \sigma^x - iJ_z \alpha^{\dagger} & J_x \sigma^y \end{pmatrix}, \quad (5)$$

where $\alpha=\text{diag}[\exp(-iq_2), -\exp(iq_1)]$, $q_1=\mathbf{q} \cdot \mathbf{n}_1$, $q_2=\mathbf{q} \cdot \mathbf{n}_2$.

The single particle spectrum $\varepsilon(\mathbf{q})=-\varepsilon(-\mathbf{q})$ is given by the eigenvalues of the spectral matrix $\tilde{G}(\mathbf{q})$. An important property of the spectrum is whether it is gapless, i.e., whether $\varepsilon(\mathbf{q})$ vanishes for some \mathbf{q} . Obviously, the vanishing of determinant $\text{Det}(\tilde{G}_{VF})$ enjoys the zero eigenvalues of \tilde{G}_{VF} . Then the gapless condition is

$$J_x^2 + J_y^2 = J_z^2. \quad (6)$$

As shown in Fig. 2(d), the phase diagram of our model consists of three phases, the gapless phase B , which is actually a conical surface, distinguishing from two gapped phases A_z and A_{xy} . Since the possible zero energy degenerate points are $(0, \pm\pi)$ and $(\pm\pi, 0)$ in the first Brillouin zone, we choose $J_x=J_y=1$, $J_z=\sqrt{2}$, and $q_1=\pi$ to plot the profile graph of the energy spectrum with respect to $q_2 \in [-\pi, \pi]$ in Fig. 3(b) by solid lines. The eigenvalues of \tilde{G}_{VF} are chosen in the concourse $\{\pm\sqrt{2} \cos(q_2/4), \pm\sqrt{2} \sin(q_2/4)\}$. Thus in the vicinity of the energy degenerate points, the low-energy excited spectrum is approximately linear. This property may be helpful to study quantum state transfer problems.¹⁷

Case II. We choose another particular direction for each link as shown in Fig. 2(b), and the plaquettes with $w_p^{(4)}=-1$ or $w_p^{(8)}=-1$ are marked by blue shadings. In this vortex-half occupied (VHO) lattice, each unit cell contains eight kinds of sites, $A_{\mathbf{q}}^{\dagger}=(a_{\mathbf{q},1}^{\dagger}, a_{\mathbf{q},2}^{\dagger}, a_{\mathbf{q},3}^{\dagger}, a_{\mathbf{q},4}^{\dagger}, a_{\mathbf{q},5}^{\dagger}, a_{\mathbf{q},6}^{\dagger}, a_{\mathbf{q},7}^{\dagger}, a_{\mathbf{q},8}^{\dagger})$, and the corresponding 8×8 spectral matrix becomes

$$\tilde{G}_{VHO} = \begin{pmatrix} J_x \sigma_y & -iJ_y \sigma_x & 0 & iJ_z e^{-iq_2'} \alpha^{\dagger} \\ iJ_y \sigma_x & J_x \sigma_y & -iJ_z \beta^{\dagger} & 0 \\ 0 & iJ_z \beta & J_x \sigma_y & -iJ_y \sigma_x \\ -iJ_z e^{iq_2'} \alpha & 0 & iJ_y \sigma_x & -J_x \sigma_y \end{pmatrix}, \quad (7)$$

where $\alpha=\text{diag}(1, -e^{-iq_1'})$, $\beta=\text{diag}(e^{-iq_1'}, -1)$, $q_1'=\mathbf{q} \cdot \mathbf{n}_1'$, $q_2'=\mathbf{q} \cdot \mathbf{n}_2'$, $\mathbf{n}_1'=(1, 1)$, and $\mathbf{n}_2'=(-1, 1)$. The gapless condition for the VHO lattice is

$$J_x^2 < J_y^2 + J_z^2, \quad J_y^2 < J_x^2 + J_z^2, \quad J_z^2 < J_x^2 + J_y^2 \quad (8)$$

and the corresponding phase graph is plotted in Fig. 2(e). We notice that the same phase graph has been obtained by Pachos⁷ for the Kitaev model.

Case III. We choose the directions of links as shown in Fig. 2(c) so that the translational symmetry still holds and $w_p^{(4)}=w_p^{(8)}=-1$ for every plaquette. The unit cell can be chosen as the same as the one in the VF sector, so do α , q_1 , and q_2 . Therefore

$$\tilde{G}_{VFO} = \begin{pmatrix} J_x \sigma^y & -iJ_y \sigma^x + iJ_z \alpha \\ iJ_y \sigma^x - iJ_z \alpha^{\dagger} & -J_x \sigma^y \end{pmatrix}. \quad (9)$$

The gapless condition is found as

$$(J_x - J_z)^2 \leq J_y^2 \leq (J_x + J_z)^2. \quad (10)$$

If $J_x, J_y, J_z \geq 0$, we have $J_x \leq J_y + J_z$, $J_y \leq J_x + J_z$, $J_z \leq J_x + J_y$. Thus in this case the phase diagram of our model is the same as that of Kitaev's honeycomb model. As shown in Fig. 2(f), the region within the red lines labeled by B is gapless. The other three gapped phases A_x , A_y , and A_z are algebraically distinct. However, the energy spectrum of the 4-8-8 mosaic model is more complex than that of the Kitaev model. When $J_x=J_y=J_z=1$ and $q_1=-q_2=q$, the eigenvalues of the single fermion are chosen in the concourse $\{-1/2 \pm \cos(q/2 + \pi/4), 1/2 \pm \cos(q/2 - \pi/4)\}$. Similarly, the different energy spectrums of mosaic spin models imply their different dynamic properties.

In order to see the stability of the ground state in the VF sector, we compare the ground energy $E_0=-\sum_{\mathbf{q}} \varepsilon_{\mathbf{q}}/2$ of the VF lattice with that of the VHO and VFO lattices mentioned above. By choosing $J_x=J_y=J_z=1$, we find the ground energy per site is $E_{0,VF}=-0.80415$, $E_{0,VHO}=-0.75930$, and $E_{0,VFO}=-0.73631$, so $E_{0,VF} < E_{0,VHO} < E_{0,VFO}$. The other cases can be studied similarly. Actually, as it was pointed out by Kitaev,² Lieb's theorem¹⁸ ensures that the VF lattice has the lowest energy to form a ground state. In the following, we will focus on the stable VF lattice and investigate the nontrivial topological properties in the B phase.

TOPOLOGICAL PROPERTIES OF B PHASE IN THE PRESENCE OF MAGNETIC FIELD

The perturbation $V=-\sum_j (h_x \sigma_j^x + h_y \sigma_j^y + h_z \sigma_j^z)$ introduced by Kitaev² can break the time-reversal symmetry. Then the nontrivial third-order term becomes $H_{eff}^{(3)}=\kappa \sum_{j,k,l} (iZ_j Z_{kl}) c_j c_k c_l$, where $\kappa \sim h_x h_y h_z / J^2$. As illustrated in Fig. 3(a), the thin

dashed arrows represent the effective second nearest-neighbor interactions between fermions induced by $H_{eff}^{(3)}$ and their directions denote the chosen gauge $Z_{jl}Z_{kl}$. When $\kappa=0.025$, the changed profiled spectrum is figured by dashed lines in Fig. 3(b). Therefore the system in the B phase acquires an energy gap in the presence of a magnetic field, which is helpful for protecting non-Abelian anyons.

According to Kitaev,² the topological properties of a two-dimensional noninteracting fermion system with an energy gap are usually characterized by Chern number, which can be determined by observing the edge modes of the spectrum.^{2,19} If the system illustrated in Fig. 2(a) is finite along the \mathbf{n}_2 direction while still periodic in the \mathbf{n}_1 direction, its energy spectrum is shown in Fig. 3(c) with $J_x=J_y=1$, $J_z=\sqrt{2}$, and $\kappa=0.025$. Then we can observe two edge modes (corresponding to two edges) crossing at $E=0$. Since the Fermi energy lies in the central gap, only these two edge states around zero energy are relevant to the Chern number.¹⁹ We also notice that the two edge modes have a universal chiral feature,² i.e., even if the edges are changed, the energy curves of the edge modes do not change their tendencies, respectively. Therefore we conclude that the Chern number is ± 1 in the non-Abelian B phase. We also get zero Chern number in the Abelian phases A_{xy} and A_z with similar studies. Compared with Kitaev's honeycomb model and the 4-8-8 mosaic model with even cycles in the lattice, the 3-12-12 mosaic model with odd cycles spontaneously breaks time

reversal symmetry to obtain Chern number ± 1 without applying a magnetic field.^{2,20}

CONCLUSION

We generalize Kitaev's honeycomb model to various mosaic spin models with translation and rotation symmetries and study the 4-8-8 case in detail. It is found that when $|J_z| \gg |J_x|, |J_y|$, our model is equivalent to Kitaev's toric code model with Abelian anyons. Different vortex excitations result in different phase diagrams with a gapless and gapped spectral structure. In the stable vortex-free case, the zero-energy Dirac points appear and the external magnetic field can induce an energy gap. The nontrivial Chern number in the B phase is obtained by studying the edge modes of the spectrum.

ACKNOWLEDGMENTS

We thank X. G. Wen, T. Xiang, Y. S. Wu, Y. Yu, H. Q. Lin, G. M. Zhang, and J. Vidal for helpful discussions. One of the authors (D.L.Z.) acknowledges the hospitality of the program on "Quantum Phases of Matter" by KITPC. The project was supported by the NSFC (Grants No. 90203018, No. 10474104, and No. 60433050) and the NFRPC (Grants No. 2006CB921206, No. 2005CB724508, and No. 2006AA06Z104).

¹X. G. Wen, *Quantum Field Theory of Many-Body Systems* (Oxford University, New York, 2004).

²A. Kitaev, *Ann. Phys. (N.Y.)* **303**, 2 (2003); **321**, 2 (2006).

³X. G. Wen, *Phys. Rev. Lett.* **90**, 016803 (2003); M. A. Levin and X. G. Wen, *Phys. Rev. B* **71**, 045110 (2005).

⁴J. Preskill, <http://www.theory.caltech.edu/people/preskill/ph229/> (2004).

⁵G. K. Brennen and J. K. Pachos, arXiv:0704.2241, *Proc. R. Soc. London, Ser. A* (to be published).

⁶S. Das Sarma, M. Freedman, C. Nayak, S. H. Simon, and A. Stern, arXiv:0707.1889.

⁷J. K. Pachos, *Int. J. Quantum Inf.* **4**, 947 (2006); *Ann. Phys. (N.Y.)* **322**, 1254 (2007).

⁸H. Bombin and M. A. Martin-Delgado, *Phys. Rev. Lett.* **97**, 180501 (2006).

⁹X. Y. Feng, G. M. Zhang, and T. Xiang, *Phys. Rev. Lett.* **98**, 087204 (2007); D. H. Lee, G. M. Zhang, and T. Xiang, arXiv:0705.3499, *Phys. Rev. Lett.* (to be published).

¹⁰H. D. Chen and J. P. Hu, arXiv:cond-mat/0702366 (unpublished);

H. D. Chen and Z. Nussinov, arXiv:cond-mat/0703633 (unpublished).

¹¹N. E. Bonesteel, L. Hormozi, G. Zikos, and S. H. Simon, *Phys. Rev. Lett.* **95**, 140503 (2005); L. Hormozi, G. Zikos, N. E. Bonesteel, and S. H. Simon, *Phys. Rev. B* **75**, 165310 (2007).

¹²Z. Nussinov and G. Ortiz, arXiv:cond-mat/0702377 (unpublished).

¹³L. Fidkowski, M. Freedman, C. Nayak, K. Walker, and Z. H. Wang, arXiv:cond-mat/0610583 (unpublished).

¹⁴N. Read and D. Green, *Phys. Rev. B* **61**, 10267 (2000).

¹⁵Y. Yu and Z. Q. Wang, arXiv:0708.0631 (unpublished).

¹⁶R. Kerner, *Topology in Condensed Matter* (Springer, Berlin, 2006), Chap. 3.

¹⁷S. Yang, Z. Song, and C. P. Sun, *Phys. Rev. A* **73**, 022317 (2006); *Eur. Phys. J. B* **52**, 377 (2006).

¹⁸E. H. Lieb, *Phys. Rev. Lett.* **73**, 2158 (1994).

¹⁹Y. Hatsugai, *Phys. Rev. Lett.* **71**, 3697 (1993); *Phys. Rev. B* **48**, 11851 (1993).

²⁰H. Yao and S. A. Kivelson, arXiv:0708.0040, *Phys. Rev. Lett.* (to be published).